Fermilab Library
0 1160 0052512 5

SDC-90-00098

SDC
SOLENOIDAL DETECTOR NOTES

A CONCEPTUAL DESIGN STUDY OF A GENERAL PURPOSE SOLENOIDAL DETECTOR FOR THE SSC

T. Doi, M. Fujita, H. Kakui, T. Kondo, K. Ogawa, T. Ohba,
I. Ohno, Y. Watanabe, A. Yamamoto

May 31, 1990

SDC-90-00098
JSD - NOTE - 1990 - 17

May 31, 1990

A conceptual design study of a general purpose solenoidal detector for the SSC

T.Doi[1], M.Fujita[1], H.Kakui[1], T.kondo[2], K.Ogawa[2], T.Ohba[1], I.Ohno[1], Y.Watanabe[3], and A.Yamamoto[2]

1)Ishikawajima-Harima Heavy Industries Co., Ltd., Tokyo, Japan
2)KEK,Laboratory for High Energy Physics, Tsukuba, Ibaraki, Japan
3)Tokyo Institute of Technology, Tokyo, Japan

ABSTRACT

This is a report on the study made on a conceptual design of a general purpose solenoidal detector for the SSC. The main issue was how to build a detector weighing about 30k tons, maximizing hermeticity while satisfying good support, easy access, enough space for cables and pipes etc. We also investigated a possibility of toroidally magnetizing iron.

1. Introduction

It is not at all trivial to construct a general purpose detector for the SSC. The size is inevitably big, weighing about 30k tons, and the requirements are stringent and are often contradicting. For example, the requirement of hermeticity is hard to satisfy, while allowing good support, easy access, space for cables and pipes etc. We felt it important to start a study of a conceptual design of a detector as a whole for the SSC at an early stage, even though none of the detector components have been decided yet. We focus our attention to common issues that arise in constructing such a detector, disregarding details of each detector component. In this study, we have simply picked reasonable values for the size and the weight of each detector component.

Main issues of the study are as follows.

1) Maximize hermeticity, while allowing sufficient mechanical strength, good support, space for cables and pipes, an easy access etc.
2) Optimize structural elements, taking into account machining, transportation, assembly etc.
3) Find implications to the design of an experimental hall.
4) Find a realistic design of iron toroids.

An interim report was given in January this year[1], and the present report is the final one, even though we have certainly not fully answered to the issues listed above.

2. Overall design considerations

We intended this study to be as general as possible to be applicable for most choices of detector components. But we had to specify a starting geometry, and we have adopted the "ACS design", where ACS stands for air core solenoid, meaning that the superconducting solenoidal coil is placed at some distance from end return yoke. This choice creates some non-uniform field in the tracking volume and leakage field outside of the solenoid, but the main advantage is that a calorimeter can be built outside of the solenoid, allowing smooth transition between barrel and endcap calorimeter, and thus allowing more hermetic calorimetry. It has been shown to be possible to construct such a magnet with 2T field with sufficiently thin material[2].

The overall design of the detector is shown in Fig.1 and Fig.2. For each detector component, we have specified its approximate size and weight as summarized in Table 1, and we have allowed reasonable space for cables and pipes. The main structure is three-layer octagonally shaped iron cylinder, whose size is about 18m in diameter and 24m in length, weighing about 22k tons. This serves both as return yoke of the inside solenoid and muon filter. This is to be directly constructed in an experimental hall, and never moves. For a purpose of study, we have investigated the possibility of magnetizing the iron. This would give an additional momentum measurement for muons and may help triggering on muons. Whether we choose to do so or not depends on the physics requirements and cost optimization. Each layer is toroidally magnetized, excited by coils wound in the axial direction at each octant. Muon chambers are placed in front, in between and at the back of the iron layers. How to install and assure the alignment of chambers is a nontrivial question requiring much harder study and has not been done here. In this design, every other detector component is installed from one of the open ends, slided along the axis as shown in Fig.3.

3. Assembly of the barrel iron structure

The choice of the octagonal shape seems to be optimum, when requirements of hermeticity, ease of assembly and the structural solidness are considered. One layer of iron is made in turn of 3 layers of iron plates. A convenient unit to transport and to handle is a hot-rolled iron plate of about 8m in length, 3m in width and 0.3m in thickness, weighing about 50 tons. All four sides of a plate are machined. One of the sides is cut and machined as shown in Fig.4, in order to support the weight of the plate directly above and to position it precisely. These plates are either bolted or welded each other in place. It is desirable to minimize the amount of welding to be done in the experimental hall, in order both to keep the hall clean and to shorten the construction period. But then, the cost of machining will go up. Thus, we must balance the two carefully.

The assembly proceeds as shown in Fig. 5. The lower half of the structure is assembled from outer to inner layers. The uppe

half is assembled using a jig shown in Fig. 6. Three layers of octagonal cylinders are separated and held in place by 15cm-thick spacers placed every 3m or so along the axis and near each apex of the octagon as shown in Fig. 7. These spacers are placed carefully such that there are no completely dead regions when looked from the interaction point to guarantee good hermeticity for the muon detection. This choice of spacers creates a problem of how to install muon chambers between two spacers. We may prefer other design of spacers, or may simply give up inserting muon chambers in between iron plates.

It is probably a good idea to use the walls of the experimental hall for the support of the whole structure. This would ease the design of the support to hold the whole detector depicted in Fig. 1. Thus the experimental hall should be made just wide enough to contain the detector. We discuss more about requirements on the experimental hall in section 6.

4. Magnetizing the barrel and endcap iron

Three layers of barrel cylinders are toroidally magnetized by winding coils as shown in Fig. 8. A coil is a hollow conductor made of copper with the cross section of 30mm by 70mm. The hole at the center is 20mm in diameter and is for water cooling. A convenient piece that allows transportation is about 12m in length and is made in extrusion technique. An inevitable consequence is that coil joints come at the half way into the barrel cylinder. Care must be taken in joining coils to keep the water path open and not to cause water leak. This can be done with a well established technique of inserting a sleeve and welding outside the joint. A joint at an end may be done as shown in Fig. 8. Coils are supported loosely so that they can slide along the axis of the cylinder, when they expand because of the heat dissipation. The height required for the coil placement is 37mm.

An endcap toroid consists of 4 layers of iron plates as shown in Fig.9. Again muon chambers are placed in front, in between and at the back of these layers. A convenient unit to handle is a trapezoidal piece made of three layers of hot-rolled iron plates, weighing about 60 tons. All of the sides are precisely machined for the purpose of accurate assembly. Four of these units are assembled first, each separated by spacers, making an octant. Then a coil is wound around these units. This choice of design, instead of e.g. assembling disk shaped iron plates, is made to obtain more uniform field by inserting wedge shaped non-magnetic material as discussed in section 8.

5. Installation and access of detector components

Once the three-layer octagonal cylinders are constructed, the other detector components are installed from one of the open ends as shown in Fig.3. As the construction of the calorimeter will take equally long time, they are assembled separately in an assembly area, which should be close to or within the

experimental hall. The completed calorimeter is moved into the beam line on a cart, then slided into the detector as shown in Fig.3.

A sliding mechanism is provided by a plastic plate called "oilless fiber freon". It has a good mechanical strength as well as a low friction coefficient as summarized in Table 2. Table 3 gives a comparison of this and an ordinary tirtank method. A pair of these plates are used as shown in Fig.10. It is clear that this sliding mechanism is well suited for this application, requiring less space for the moving mechanism. When an access-need arises to an inner detector component, the outer components are slided out and put aside if necessary.

6. Implications to an experimental hall

We assume that an experimental hall is about 100m below ground. A possible design of an experimental hall is shown in Fig.11. As the cost to dig an experimental hall increases linearly with the area to be excavated[2], the area needed for assembly, maintenance and drop hatch is all to be fit in along the beam line. We discarded the original idea of having an assembly area perpendicular to the beam line for the sake of cost saving. A drop hatch is about 10m by 10m. The space needed for the assembly area will depend on the choice of calorimeter technique and has to be optimized taking into the excavation cost as well. The design of the support that holds the whole structure would simplify greatly, if the walls of the hall can be used for the support as well. For the crane capability, we need at least two cranes of about 100 ton each for a parallel effort of assembly work. Utility area depends on the type of the detector technology chosen, but a good size area near the detector is surely needed.

7. Structural analysis

A structural analysis of the iron structure was done with a program MSC/NASTRAN, a standard program for a finite element method. In modeling three-layer iron plates of an octagonally shaped cylinder, each layer of iron plates are allowed to slide. This approximation certainly gives an overestimation for the deformation. Thus the integrity of the structure is proven if the calculated stresses are within the allowed value. The calculated deformation due to the self-weight of the barrel cylinder is shown in Fig. 12. The maximum is at the top, amounting to 0.8mm. It is essential that the structure is supported also from both sides. The amount of deformation due to the weight of the inside detector is smaller as shown in Fig. 13. Probably, we do not have to worry about earthquakes in Texas, but we also calculated the effect by applying a side way static force of 0.2g. The result due to the self-weight is shown in Fig.14, where the maximum deformation is seen to occur also at the top. Figure 15 shows the effect due to the weight of the inner detector. Table 4 shows the calculated stresses at various points. They are well within the allowed stress for iron.

8. Calculation of the toroidal field

Magnetic field within iron is calculated using mostly a program called JMAG2D, which allows field calculation of two dimensional configuration. Some checks were made with three dimensional calculation using JMAG3D, whose results agreed well with that of two dimensions. The calculation utilizes the symmetry of the system. For the barrel part, a 1/16 section is enough for the calculation. Figure 16 explains the mesh size for the calculation and the notation of the coil placement. For iron material, special grade suited for magnetic application is selected, and compared with normal grade, SS41. The B-H curves for the two materials are shown in Fig. 17. From this figure alone, it is seen to be increasingly difficult to obtain higher field. For example, it requires three to five more currents (or power) to obtain 2T field instead of 1.8T field.

A result of calculation for the barrel toroid is shown in Table 5. The coil placement at the center of each octant seems to be good enough for the uniformity of the field. Figure 18 shows the field obtained vs. the number of amp-turns necessary for the third layer, as a typical example. As the power required to excite the coil increases rapidly beyond the field of about 1.8T, it is nontrivial to obtain higher field. There, the difference between special and normal grade of iron seems to diminish. The return flux of 2T solenoid field gives little influence to the toroidal field.

For the endcap toroid, it is well known that the field is the highest at the smallest radius, decreasing rapidly toward larger radius. Because of saturation, the deviation from the well known 1/r dependence is rather large, but the field at the outermost radius is still rather low as seen in the first row of Table 6. One way to increase the uniformity is shown in Fig.19, where a wedge shaped non-magnetic material (SUS304) is inserted to push out the field. Note that the non-magnetic material acts as a vacuum for the field calculation, but we need the same thickness of absorber material for the purpose of muon detection. The toroidal field is continuous enough to create little azimuthal dependence of the field. Results are summarized in Table 6. A uniformity within a few percent can be achieved. Figure 20 shows the field vs. amp-turns for two typical thicknesses of nonmagnetic material.

Table 7 summarizes the calculation of the heat dissipation of the coil. By using a copper coil with cross section of 30mm by 70mm, the total power consumption is limited to about 3MW for 1.8T field. As expected, most of the power is consumed in the barrel toroid, we have to optimize the requirements of physics and cost limitation to decide whether or not to magnetize the barrel part. Cooling is provided by flowing water through 20mm diameter hole bored at the center of a coil. The allowed pressure drop and the temperature rise are 5atm and 10°C, respectively. Table 8 summarizes the result of calculation for the cooling. It is well within the reasonable range.

9. Summary

This is a report on the study we have made on a conceptual design of a general purpose detector for the SSC.

The main part, the octagonal 3-layer iron cylinder has to be built directly at an experimental hall. A part of support should be provided from the walls of the experimental hall. Every other detector components are slided from one of the open ends. A good way to provide the sliding mechanism is to use a pair of plastic plates "oilless fiber freon".

Barrel and end cap iron can be magnetized up to 1.8T field, where the power consumption is 3MW. The field in the endcap iron can be made fairly uniform by inserting non-magnetic material. Obtaining higher field is increasingly difficult.

Implications to the design of an experimental hall are derived, such as the size of the hall, the assembly hall, the crane requirements etc.

ACKNOWLEDGEMENTS

The authors would like to express their sincere gratitude to Prof. S. Mori, who encouraged them to pursue this work. They are indebted to many people who injected good ideas here and there in this work.

REFERENCES

Ref. 1 "Status report on a conceptual design study of a hermetic detector for the ssc", T. Doi et al, in "Design Studies and Detector R&D for Super High Energy Hadron Colliders in Japan", March 1990, edited by T.Ohsugi and T.Kondo.

Ref. 2 "Short solenoid design", talk by A.Yamamoto, this workshop proceedings.

Ref. 3 "A solenoid detector design", talk by R.Kadel, this workshop proceedings.

FIGURE CAPTIONS

Fig. 1. Overall design of the detector ;bird's eye view.

Fig. 2 Cross sectional views of the detector.

Fig. 3. Installation of detector components.

Fig. 4. Assembly of an octagonal cylinder and a unit iron piece.

Fig. 5. Assembly of the barrel cylinder.

Fig. 6. A jig to assemble the upper part of the cylinder.

Fig. 7. Placement of spacers.

Fig. 8. Design and placement of coils for barrel and endcap toroids

Fig. 9. Assembly of an endcap toroid.

Fig.10. Sliding mechanism using a pair of plastic "oilless fiber freon".

Fig.11. Layout of an experimental hall, areas for assembly, maintenance and utility and a drop hatch.

Fig.12 Deformation of barrel cylinder due to the self-weight.

Fig.13 The same due to that of the inner detector.

Fig.14 The same due to a side way force of 0.2g (self-weight only)

Fig.15 The same as above due to the weight of the inner detector.

Fig.16. Mesh division for the calculation of the barrel toroidal field and the positioning of coils.

Fig.17 B-H curves of normal and special grade steel plates.

Fig.18. Magnetic field calculated vs. amp-turns for barrel toroid (for the third layer).

Fig.19 Mesh division for the calculation of the endcap toroidal field.
A method to increase the field uniformity by inserting a wedge-shaped non-magnetic material(SUS304).

Fig.20. Magnetic field calculated vs. amp-turns for endcap toroid with SUS304.

Table 1a Parameters of detector components (barrel part)

Element	material	shape	size(m) Rmin	Rmax	Zmax	weight (tons)	supported by
tracking	Al etc.	Cyl.	0.2	1.65	2.5	3	calorimeter
solenoid	Al etc.	Cyl.	1.7	1.95	3.8	15	calorimeter
calorimeter	Pb-LA?	Cyl.	2.0	4.50	3.8	2900	mu-filter
mu chamber	Al etc.	Oct.	4.5	5.0	11.85	45	" "
mu-filter	pure Fe	Oct.	5.0	5.85	"	6100	" "
mu chamber	Al etc.	Oct.	5.85	6.0	"	25	" "
mu-filter	pure Fe	Oct.	6.0	6.85	"	7200	" "
mu chamber	Al etc.	Oct.	6.85	7.0	"	25	" "
mu-filter	pure Fe	Oct.	7.0	7.85	"	8300	" "
mu-chamber	Al etc.	Oct.	7.85	8.35	"	120	" "

Table 1b Parameters of detector components (an endcap part)

Element	material	shape	size(m) Rmin	Rmax	Zmin	Zmax	weight (tons)	supported by
calorimeter	Pb-LA?	Cyl.	0.4	4.0	4.0	7.0	1300	mu-filter
mu-chamber	Al etc.	Oct.	0.7	4.3	7.0	7.5	40	"
toroid	pure Fe	Oct.	0.75	"	7.5	8.35	630	"
mu-chamber	Al etc.	Oct.	0.85	"	8.35	8.5	20	"
toroid	pure Fe	Oct.	"	"	8.5	9.35	630	"
mu-chamber	Al etc.	Oct.	0.95	"	9.35	9.5	20	"
toroid	pure Fe	Oct.	"	"	9.5	10.35	630	"
mu-chamber	Al etc.	Oct.	1.05	"	10.35	10.5	20	"
toroid	pure Fe	Oct.	"	"	10.5	11.35	630	"
mu-chamber	Al etc.	Oct.	"	"	11.35	11.85	40	"

Table 2 Physical properties of "oilless fiber freon"

strength	
tensile force	>1000 kgf/cm
compress force	>2000 "
impact (Idot method)	>18 cm/cm
hardness	>80HRM
Young's modulus	$>6 \cdot 10^4$ kgf/cm
Thermal properties	
expansion coefficient	$2 \sim 3 \cdot 10^{-5}$ /°C
conductivity	$4 \sim 7 \cdot 10^{-4}$ cal/sec/°C/cm
sliding coefficient of friction	
static	0.08~0.09
dynamic	0.03

Table 3 Comparison of two sliding mechanisms
tirtank vs. "oilless fiber freon"

item	tirtank	"oilless fiber freon"
coefficient of friction	excellent (0.04~0.02)	good (0.08~ 0.03)
space needed for installation		
along the axis	impossible	excellent
width	good(>300mm)	excellent(110mm)
fore-treatment	greasing	none
deterioration	rust	none
overall evaluation	poor (compact tirtank must be developed)	good (need more power to move but o.k.)

Table 4 Calculated stresses

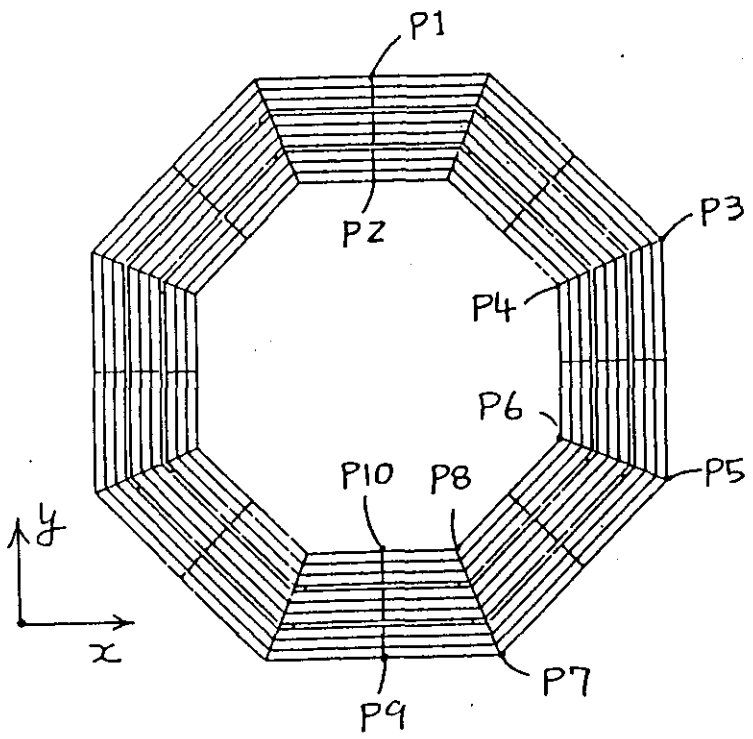

Points where stresses are evaluated

unit : kg/mm²

point \ weight		SELF-WEIGHT	SELF-WEIGHT +0.2g VERTICAL	SELF-WEIGHT +0.2g HORIZ.
P 1	inner	0.21	0.23	0.21
	outer	-0.31	-0.33	-0.31
P 2	inner	0.43	0.48	0.45
	outer	-0.17	-0.18	-0.17
P 3	inner	-0.46	-0.52	-0.58
	outer	0.44	0.48	0.54
P 4	inner	-1.62	-1.78	-1.99
	outer	1.44	1.58	1.81
P 5	inner	-0.32	-0.34	-0.39
	outer	0.22	0.24	0.27
P 6	inner	0.78	0.87	1.91
	outer	-0.94	-1.03	-2.03
P 7	inner	-0.33	-0.37	0.05
	outer	0.17	0.19	-0.05
P 8	inner	1.83	2.00	2.19
	outer	-2.11	-2.32	-2.45
P 9	inner	-0.52	-0.57	-0.51
	outer	0.38	0.41	0.37
P 10	inner	-0.56	-0.62	-0.55
	outer	0.28	0.30	0.29

allowed stress
(special grade steel) = 6.6kg/mm²

Table 6 Calculated field (endcap) (SUS inserted)

No.	coil pos.	SUS width (mm)	Lower part			Middle			Upper part			
			15000AT			——			15000AT			
			Bc (25)	Bo (30)	Be (34)	Bc (85)	Bo (90)	Be (94)	Bc (135)	Bo (140)	Be (144)	
1	A	0	2.159	(+0.32) 2.166	(+0.79) 2.176	1.985	(-3.27) 1.920	(-11.34) 1.760	1.950	(-5.38) 1.845	(-21.33) 1.534	J3887
2	A	50	0.595	(-5.21) 0.564	(-14.96) 0.506	1.109	(-0.09) 1.108	(-0.45) 1.104	1.337	(+16.08) 1.552	(+47.79) 1.976	J4037
3	A	20	1.279	(-2.35) 1.249	(-6.49) 1.196	1.469	(+1.16) 1.486	(+5.92) 1.556	1.520	(+11.45) 1.694	(+29.34) 1.966	J3864
4	A	10	1.840	(-0.71) 1.827	(-1.79) 1.807	1.779	(-0.89) 1.765	(-0.73) 1.766	1.778	(+0.62) 1.789	(+5.51) 1.876	J4422
5	A	10	1.798	(-0.72) 1.785	(-1.84) 1.765	1.718	(-0.81) 1.704	(-1.16) 1.698	1.717	(+0.35) 1.723	(+5.36) 1.809	J6417

note 1; No. 1 - 4; for special grade, No.5; normal grade (SS41).

note 2; ( ) indicates the uniformity of field in %

Table 8 Cooling characteristics of coil

No.	symbol	unit	endcap	称		
				1st layer	2nd layer	3rd layer
1	P	M W	0.195	0.738	0.922	1.107
2	m	ℓ / S	4.7/8	17.8/32	22.2/32	26.7/32
3	D	m	0.02	0.02	0.02	0.02
4	L	m	115	110	135	160
5	U	m / S	1.870	1.771	2.208	2.656
6	R e	—	5.36×10^4	5.07×10^4	6.32×10^4	7.61×10^4
7	Δ P	MPa	0.208	0.181	0.326	0.534
8	No. lines		8	32	32	32

symbols

P ; heat dissipation(W)

m ; flow rate (l/m)

D ; tube dia.(m)

L ; total length(m)

U ; velocity(m/s)

Re ; Reynolds number

ΔP ; Press. loss (Pa)

---

the formula for the pressure loss is given by;

$$\Delta P = \frac{L}{D} \cdot \frac{\rho}{2} \cdot U^2 \times 0.3164 \times \frac{1}{Re^{0.25}}$$

$$Re = \frac{U \cdot D}{\nu}$$

assumptions

	inlet	outlet
pressure	7 atm.	2 atm.
temperature	30°C	40°C

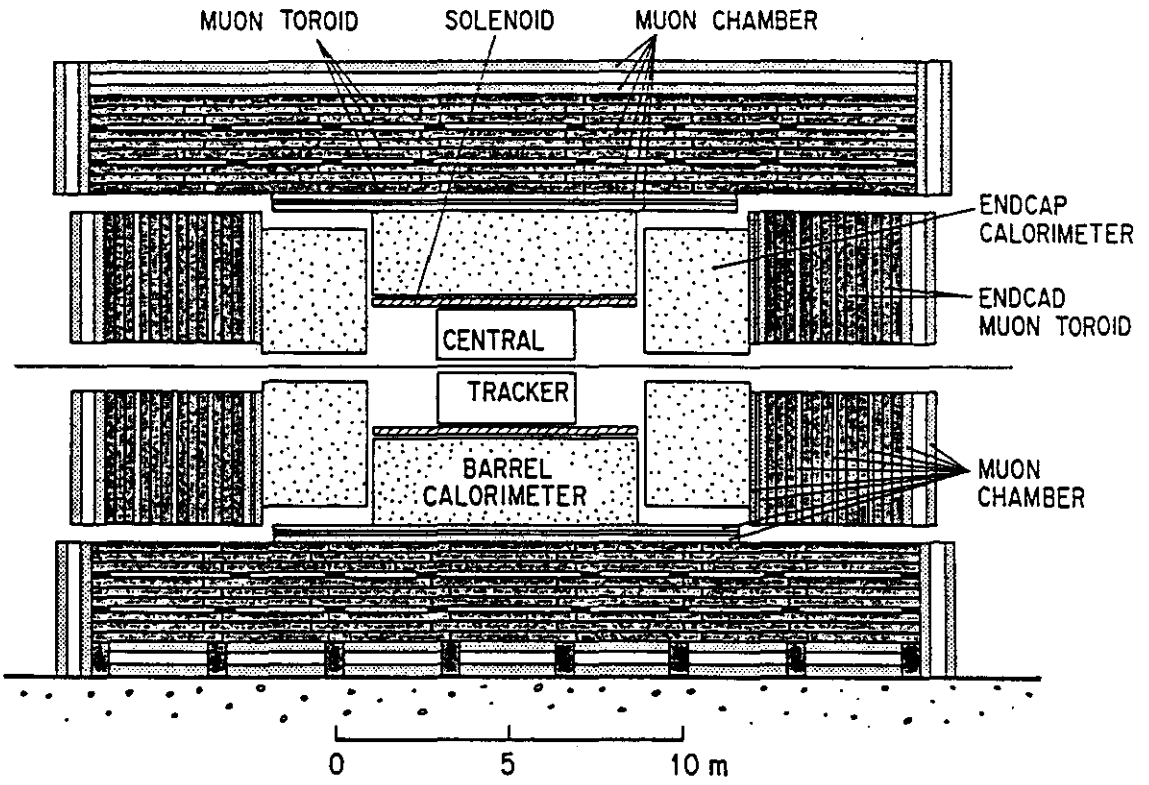

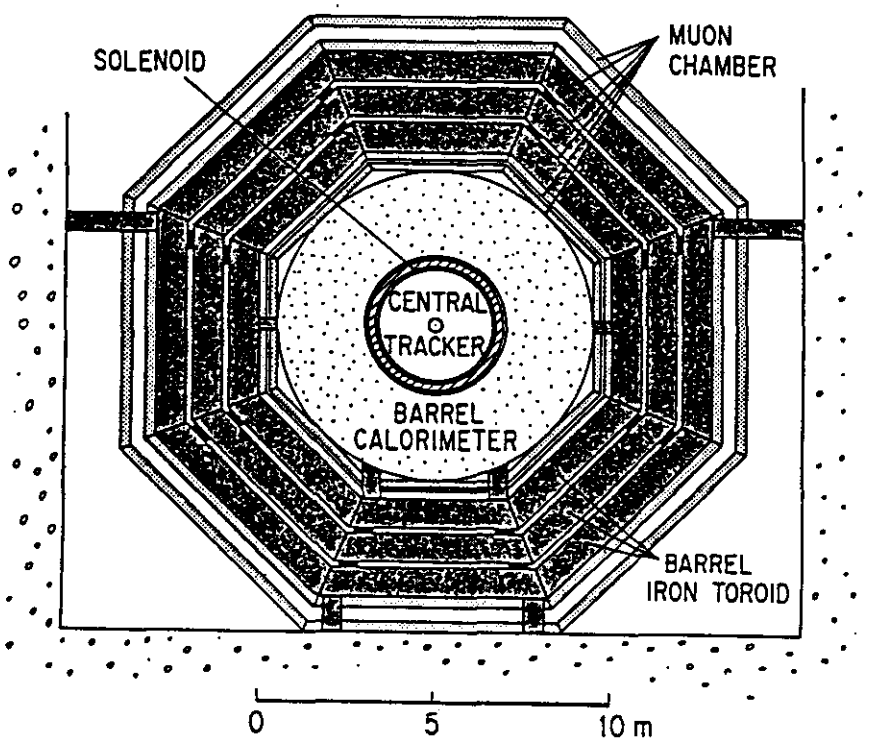

Fig. 2 Cross sectional views of the detector.

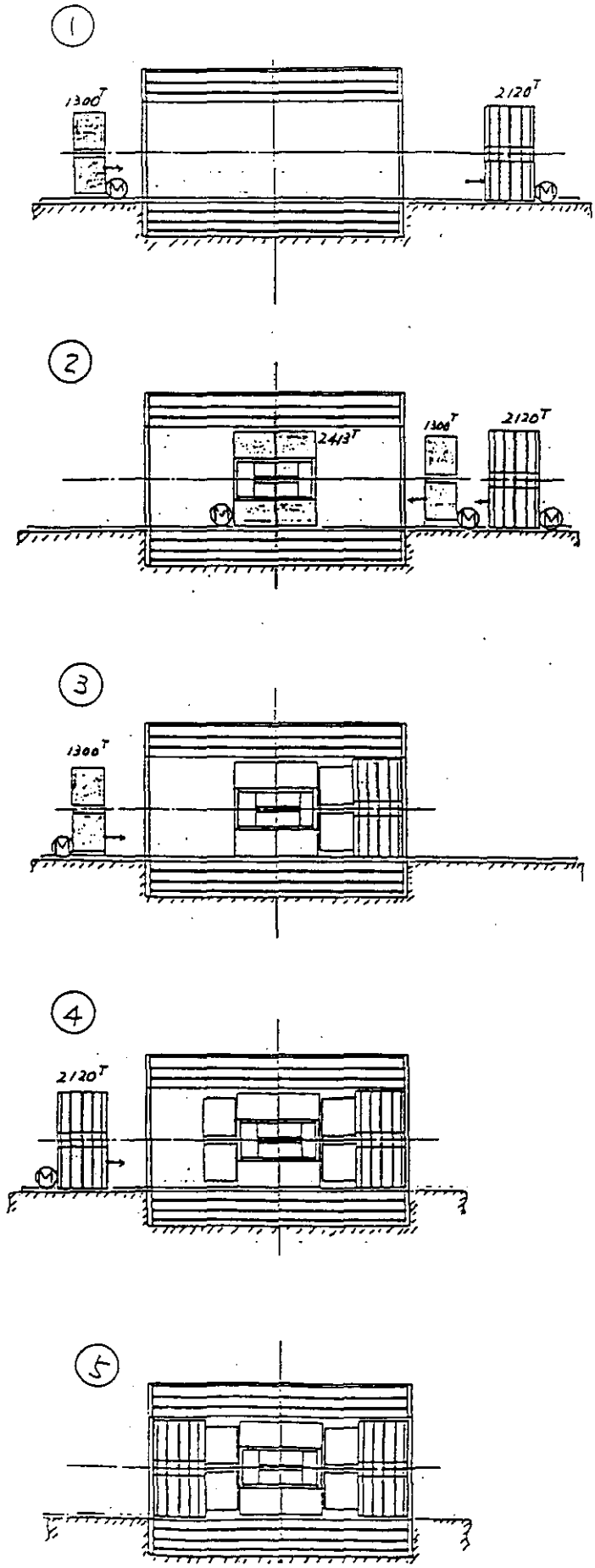

Fig. 3. Installation of detector components.

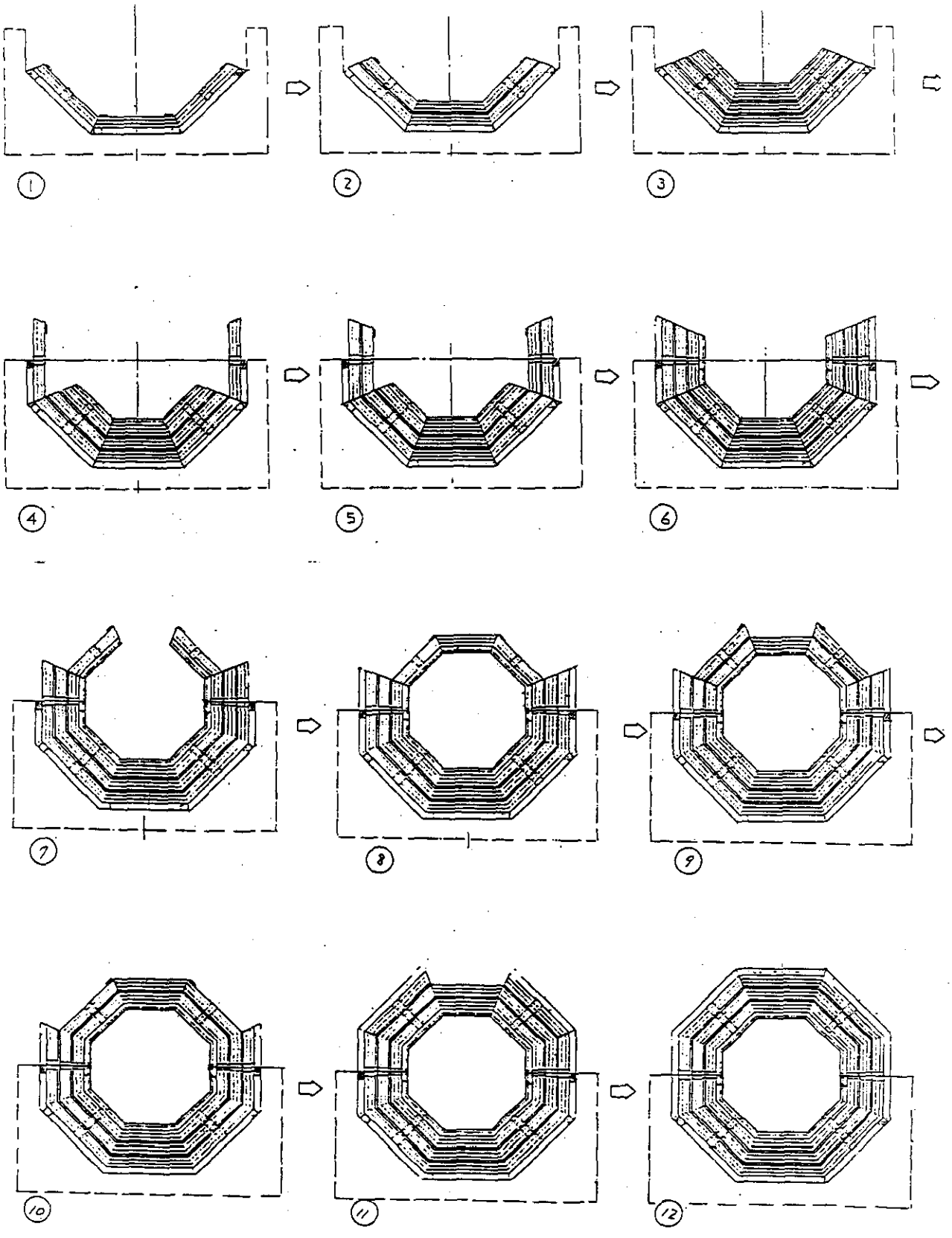

Fig. 5. Assembly of the barrel cylinder.

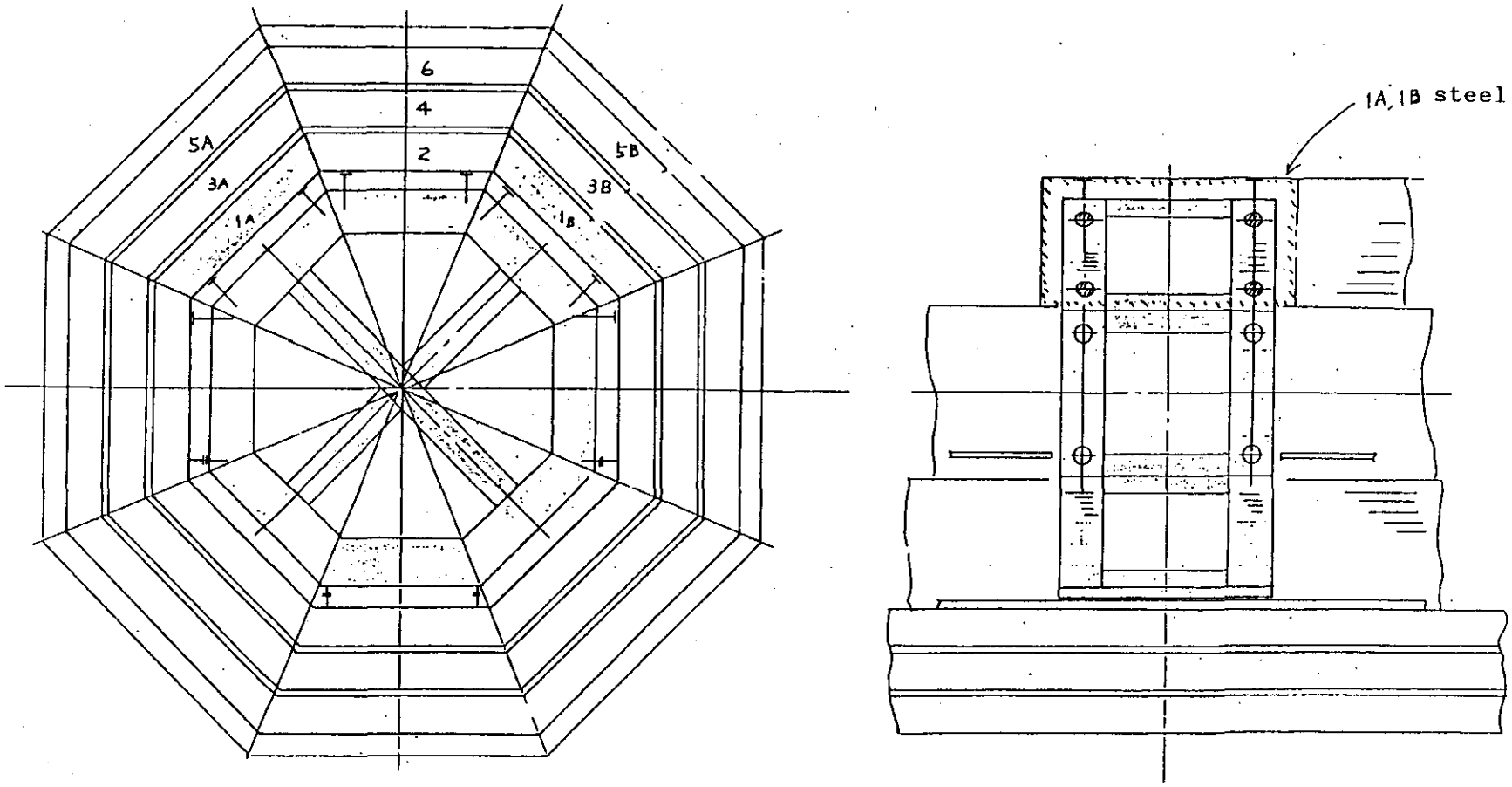

Fig. 6. A jig to assemble the upper part of the cylinder.

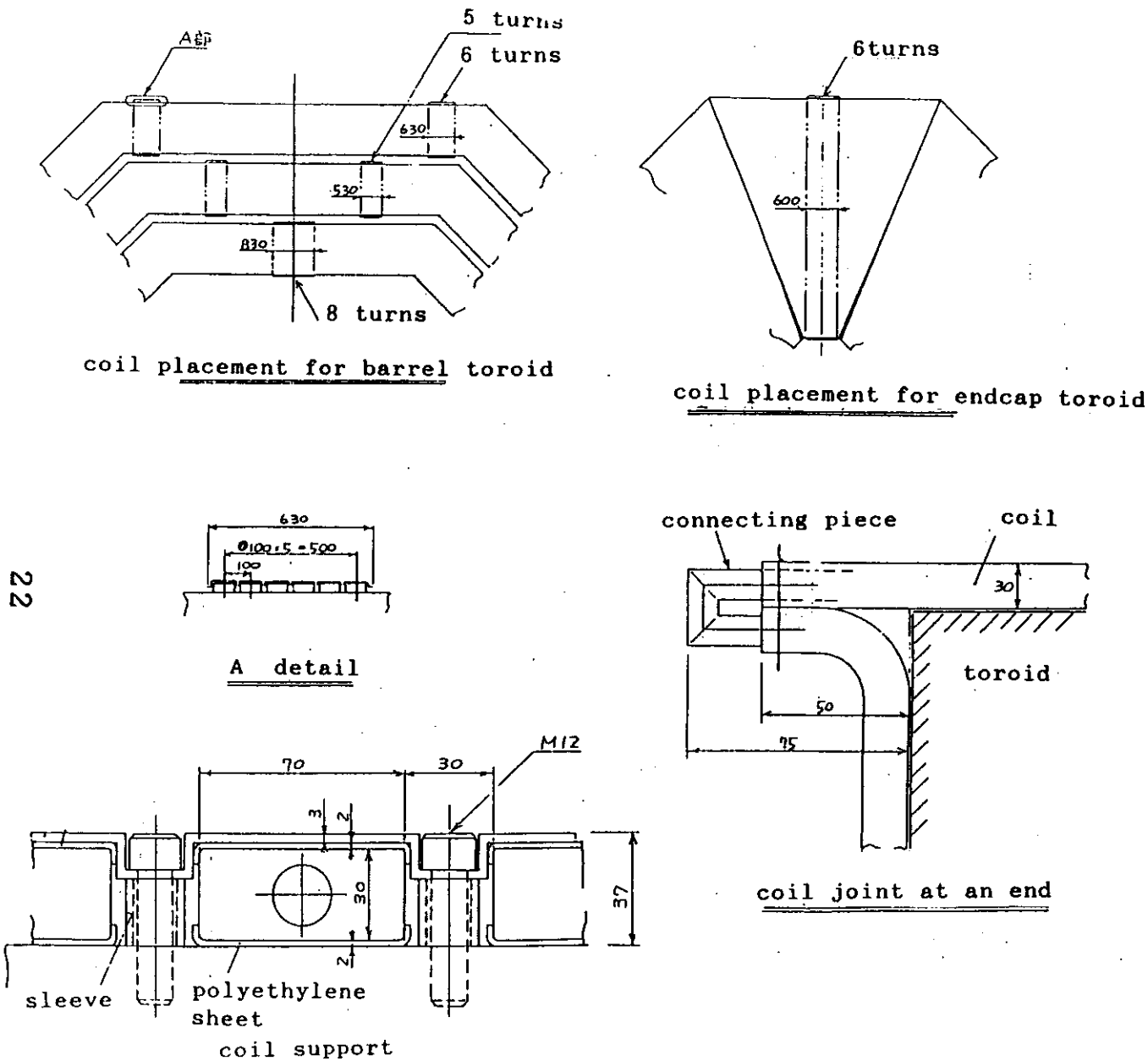

Fig. 8. Design and placement of coils for toroidal magnet.

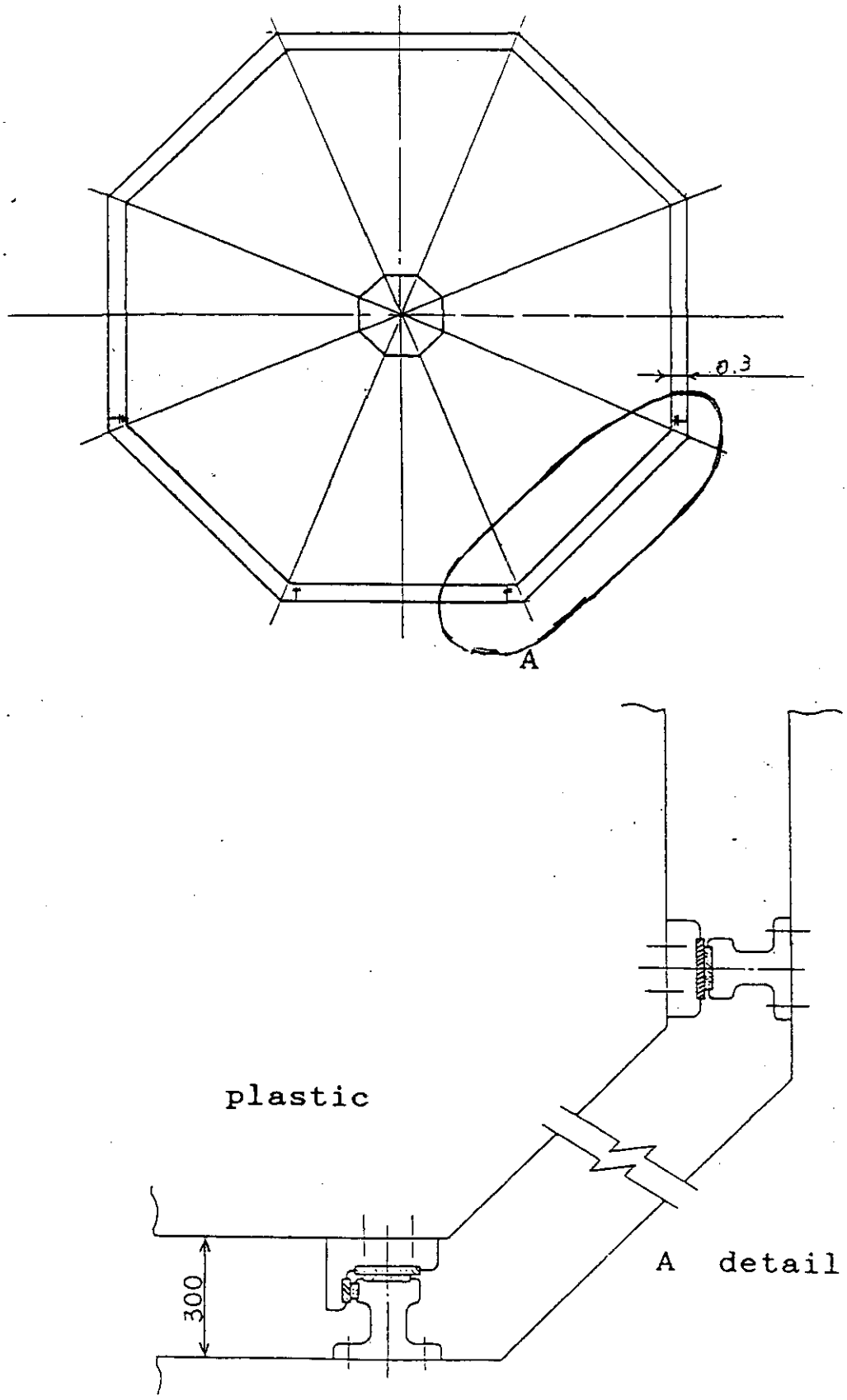

Fig.10. Sliding mechanism using a pair of plastic "oilless fiber freon".

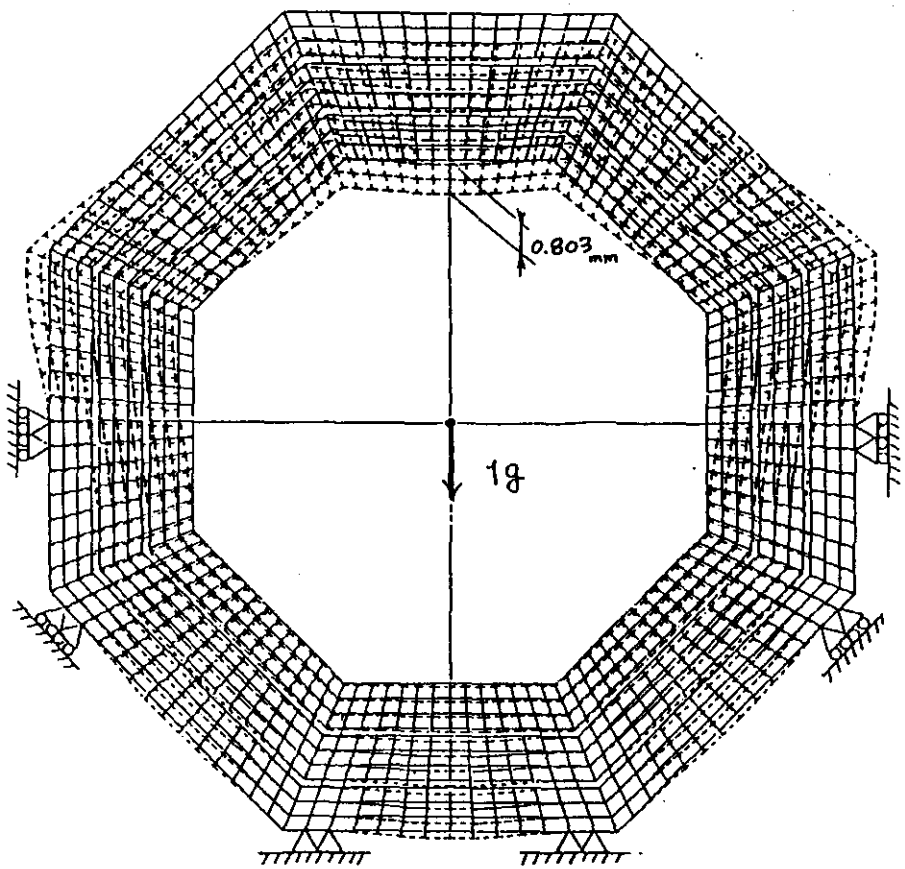

Fig.12 Deformation of barrel cylinder due to the self-weight.

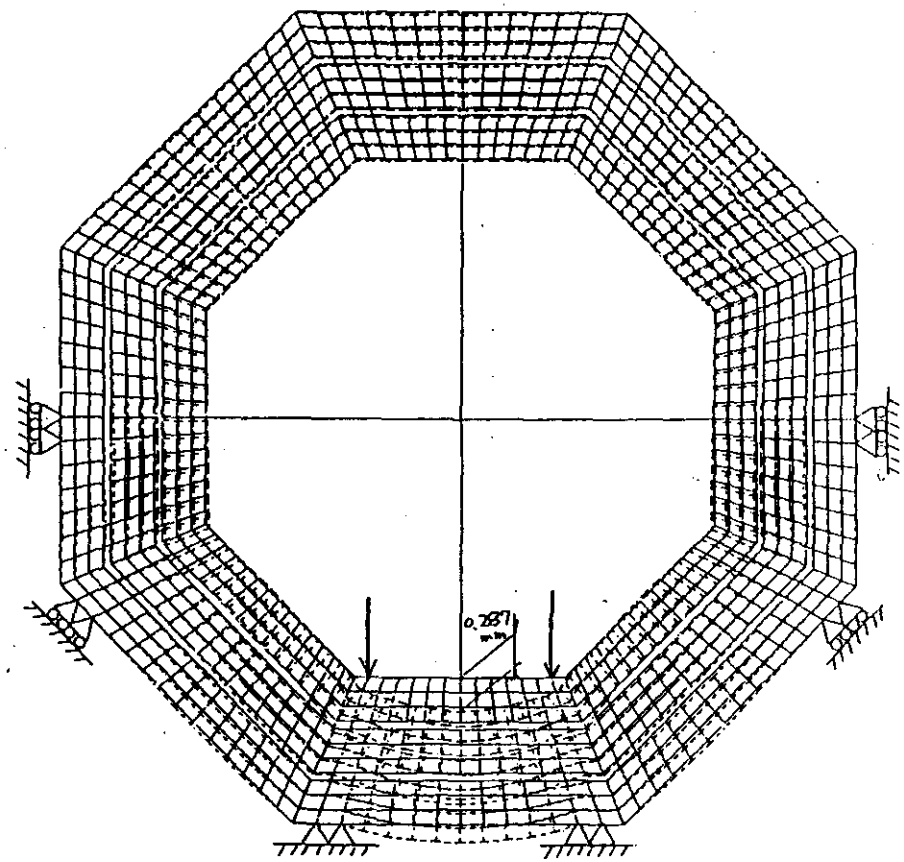

Fig.13 Deformation of barrel cylinder due to the weight of the inner detector.

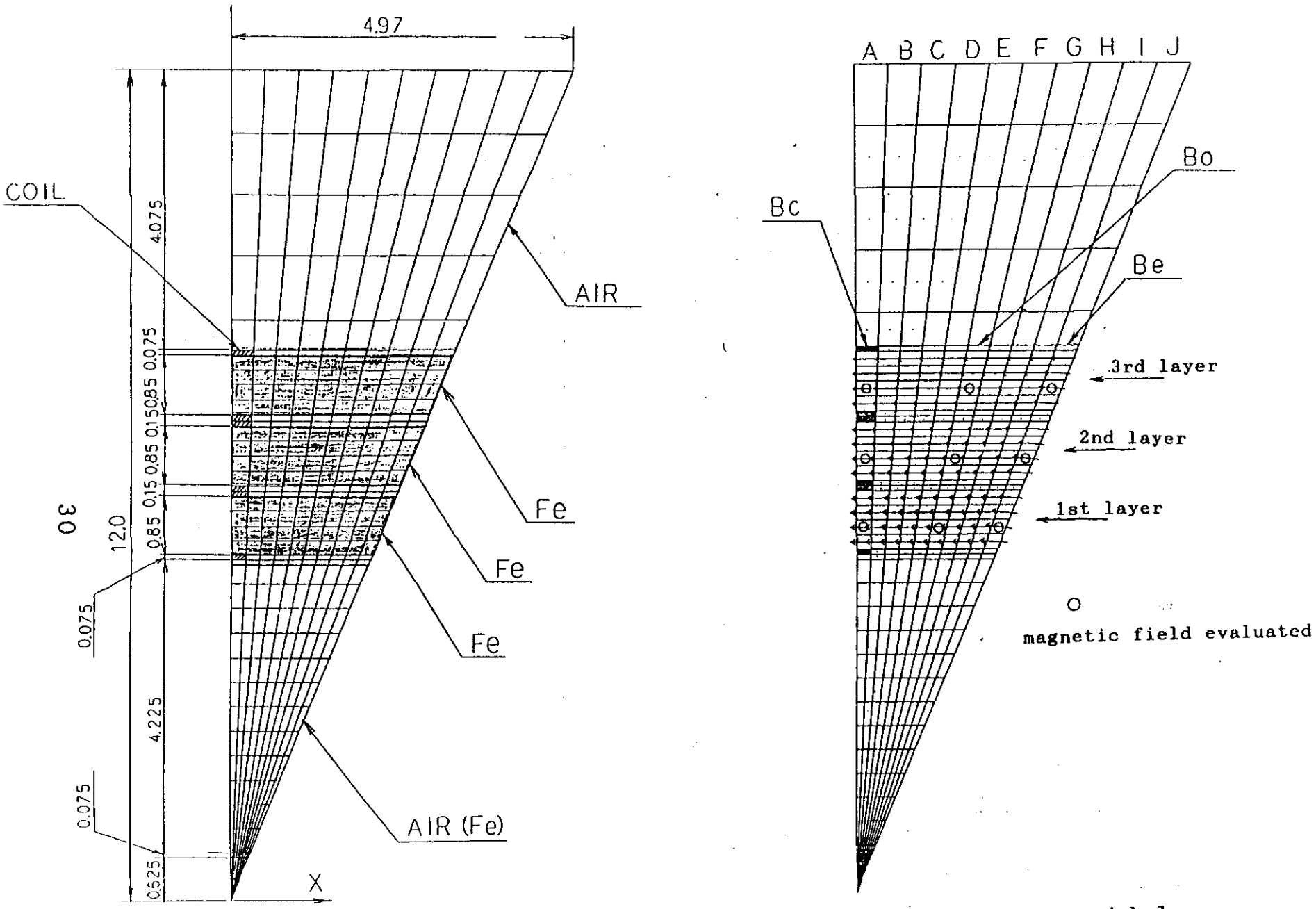

Fi(6. Mesh division for the calcu(ion of the barrel toroidal field and the positioning o(oil.

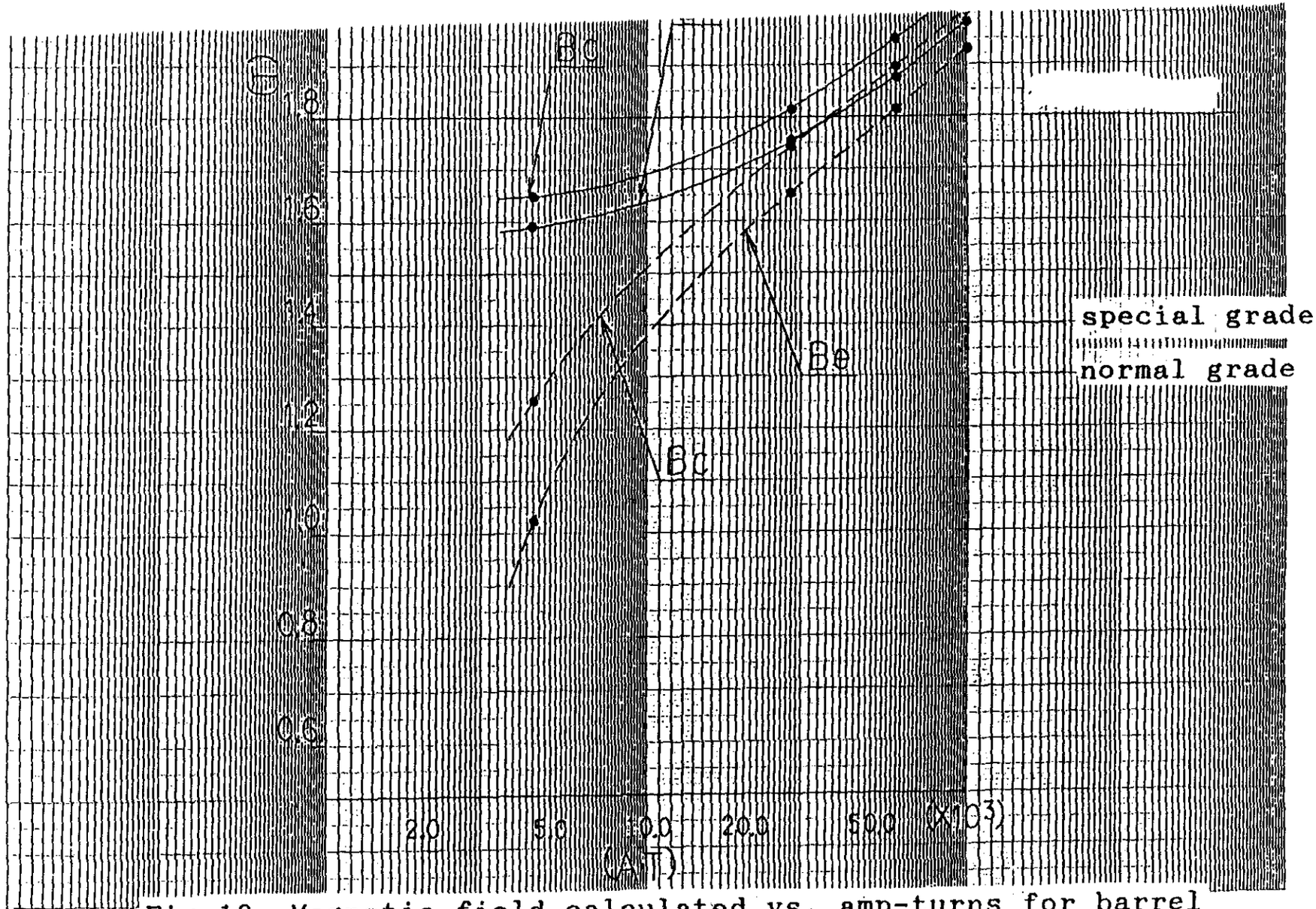

Fig.18. Magnetic field calculated vs. amp-turns for barrel toroid (for the third layer).

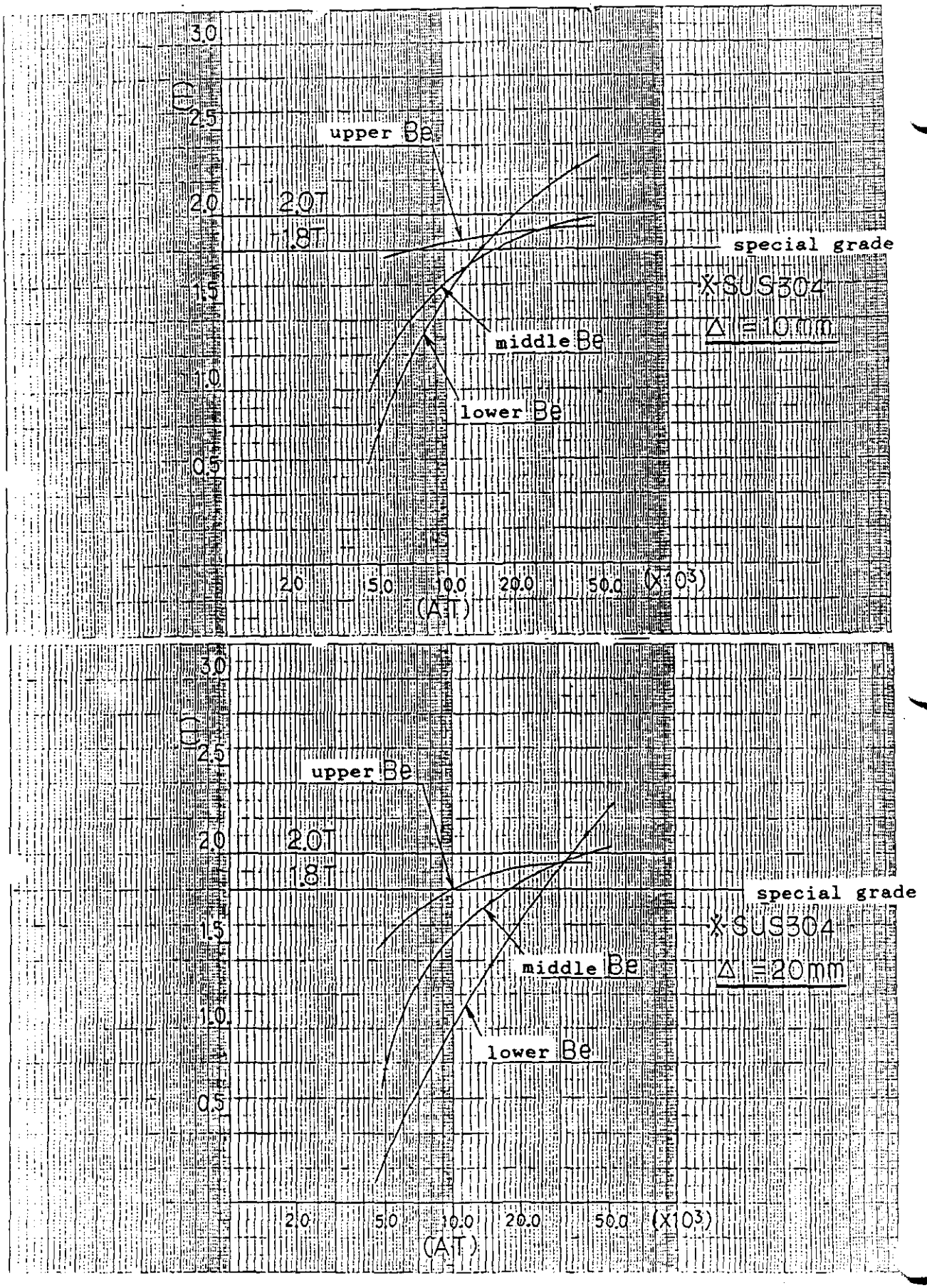

Fig.20. Magnetic field calculated vs. amp-turns for endcap toroid with SUS304.